# Signature of sterile species in atmospheric neutrino data at neutrino telescopes

**Sandhya Choubey**[⋆]

*Harish-Chandra Research Institute,*
*Chhatnag Road, Jhunsi, Allahabad 211019, India*

## ABSTRACT

The MiniBooNE results have still not been able to comprehensively rule out the oscillation interpretation of the LSND experiment. So far the so-called short baseline experiments with energy in the MeV range and baseline of few meters have been probing the existence of sterile neutrinos. We show how signatures of these extra sterile states could be obtained in TeV energy range atmospheric neutrinos travelling distances of thousands of kilometers. Atmospheric neutrinos in the TeV range would be detected by the upcoming neutrino telescopes. Of course vacuum oscillations of these neutrinos would be very small. However, we show that resonant matter effects inside the Earth could enhance these very tiny oscillations into near-maximal transitions, which should be hard to miss. We show that imprint of sterile neutrinos could be unambiguously obtained in this high energy atmospheric neutrino event sample. Not only would neutrino telescopes tell the presence of sterile neutrinos, it should also be possible for them to distinguish between the different possible mass and mixing scenarios with additional sterile states.

[⋆]email: sandhya@mri.ernet.in

# 1    Introduction

Last few years have seen a tremendous progress in the field of Neutrino Physics, so much so that its fair to say that neutrinos have now become a pivot in our understanding of physics beyond the standard model of particle physics. The first conclusive prove of the existence of neutrino mass and mixing came from the observation of atmospheric neutrinos by the SuperKamiokande detector [1]. The zenith angle dependent data on atmospheric neutrinos from this experiment could be explained only if neutrinos oscillate with $\Delta m_{31}^2 \simeq 2.1 \times 10^{-3}$ eV$^2$ and $\sin^2 2\theta_{23} = 1$. This was followed by the spectacular results on solar neutrinos from the SNO experiment, which proved beyond doubt that solar neutrinos do indeed oscillate, corroborating the observations of all earlier solar neutrino experiments, the Homestake, SAGE, GALLEX/GNO, Kamiokande and SuperKamiokande [2]. The so-called Large Mixing Angle (LMA) solution emerged as the only solution of the solar neutrino deficit problem with $\Delta m_{21}^2 = 6 \times 10^{-5}$ eV$^2$ and $\sin^2 \theta_{12} = 0.31$ [3]. The LMA solution was confirmed by the KamLAND reactor antineutrino experiment [4] and the combined solar and KamLAND data choose $\Delta m_{21}^2 = 8 \times 10^{-5}$ eV$^2$ and $\sin^2 \theta_{12} = 0.31$ as the best-fit parameter values [3]. The SuperKamiokande atmospheric neutrino results were affirmed by two terrestrial accelerator-based experiments – K2K [5] and MINOS [6] and the combined atmospheric and accelerator data demand $\Delta m_{31}^2 = 2.4 \times 10^{-3}$ eV$^2$ and $\sin^2 2\theta_{23} = 1$ [3]. Another very important result we have is from the reactor antineutrino experiment Chooz [7]. Results of this experiment, analyzed along with the other neutrino data impose the constraint that $\sin^2 \theta_{13} < 0.04$ at $3\sigma$ C.L. [3].

The latest addition to the repertoire of experimental result on neutrinos comes from the Mini-BooNE experiment [8]. The MiniBooNE experiment was set-up to reconfirm the positive oscillation signal reported by the LSND collaboration [9], which so-far remains the only experiment to have seen neutrino oscillations at a frequency which demands $\Delta m^2$ in the eV$^2$ range. All other short baseline experiments [10] have been consistent with the hypothesis of null oscillations. The MiniBooNE experiment also reported to have not seen oscillations in the energy regime consistent with LSND. The extra mass squared difference demanded by the LSND signal can be accommodated along with solar and atmospheric neutrino results only if there were sterile neutrinos. The most economical scenario comes from adding just one extra sterile neutrino, giving the so-called 2+2 and 3+1 neutrino mass schemes [11]. It has been shown that the 2+2 spectrum is strongly disfavored from the solar and atmospheric neutrino data. The 3+1 scheme on the other hand suffers from a strong tension between the positive signal at LSND and null signal in all other short baseline experiments. The addition of the MiniBooNE results puts even stronger constraints on the 3+1 picture, disfavoring it at a very high C.L. [12]. Adding two extra sterile neutrino would give us the so-called 3+2 neutrino mass spectrum [13, 14, 15]. This picture interestingly gives a reasonable explanation of all neutrino oscillation data including LSND and MiniBooNE, if CP violation is allowed [12]. In [16] the author find a very good fit to world neutrino data for a CP conserving 3+2 mass spectrum as well.

The situation concerning sterile neutrinos therefore seems to be far from settled. MiniBooNE was especially designed to confirm or refute the LSND signal and they have reported to have contradicted the LSND claim of positive oscillation signal. However, their first data set is with neutrinos while LSND had seen oscillations of antineutrinos. In addition the entire event sample

of MiniBooNE is not yet fully understood. They have seen excess electron events in their low energy sample, which still remains unexplained. It is hoped that this systematic excess of electron events seen in the experiment will eventually be explained. MiniBooNE is also now running in the antineutrino channel and results from this data set might settle the issue regarding the mismatch between the LSND and MiniBooNE results.

Resolution of this perplexing issue could also come from other kind of experiments. Presence of sterile neutrinos would lead to distinctive features in the resultant supernova neutrino signal in terrestrial detectors such as future megaton water Čerenkov detectors and neutrino telescopes like IceCube [14]. Very recently it has been shown that the planned and up-coming next generation reactor neutrino experiments such as Double Chooz, Daya Bay, Angra, and RENO, which are being built to probe the mixing angle $\theta_{13}$, could also check for the existence of sterile neutrinos through combination of data from the near and far detectors [17]. Not only should it be possible to cross-check the 3+2 neutrino mass scheme at these experiments, we should also be able put limits on the mixing angles involving sterile neutrinos [17]. Possibility of observing sterile neutrinos in the upcoming accelerator-based long baseline experiments was studied very recently in [18] for the conventional CNGS experiment, and in [19] for the future neutrino factory. In another recent paper we have shown that the existence of sterile neutrinos could in principle also be probed in the ultra high energy neutrino signal in the neutrino telescopes [20].

In this paper we show how the data from very high energy atmospheric neutrinos in neutrino telescopes such as IceCube [21], Km3Net [22], NEMO [23] and NESTOR [24] could be used to check if sterile neutrinos indeed exist. The neutrino telescopes will have energy threshold of about 100 GeV and are designed to observe ultra high energy neutrinos. The very high energy atmospheric neutrinos with energy in the range $10^{-1} - 10^4$ TeV will also be observed in these detectors and they will in principle constitute the "background" for the ultra high energy neutrino "signal". However, this atmospheric neutrino "background" in km$^3$ neutrino telescopes will be sizable and can hence be used to provide crucial information on some physics issues. The AMANDA experiment has already observed the high energy atmospheric neutrinos, and the observed flux is reported to be consistent with the theoretical predictions [25]. In 10 years of operation, IceCube will be able to collect $7 \times 10^5$ atmospheric muon neutrino events [26]. With such a huge data sample, it was shown in [26] that the atmospheric neutrino events in IceCube could be used to put severe constraints on non-standard physics. Feasibility studies of constraining non-standard physics in ANTARES was performed in [27]. We will show that for the mass squared difference needed to explain LSND, we expect near-resonant matter effects between the active and sterile neutrino states inside the Earth. This leads to drastic changes in the expected flux at the detector. This change is both energy as well as zenith angle dependent and should provide foolproof signal for the existence of sterile neutrinos in this mass regime.

The paper is organized as follows. In Section 2 we discuss the enhancement of neutrino mixing and oscillations from the matter effects due to the extra sterile states. The numerically calculated exact oscillation probabilities for the PREM matter density profile of the Earth is presented in Section 3 for the simpler (though disfavored) 3+1 spectrum. We reiterate that we present results for this case purely for illustration only. With the 3+1 exemplary case, we hope to highlight some of the features of the active-sterile resonant matter effects. In section 4 we show the oscillation probabilities for the more realistic 3+2 neutrino mass spectrum. We make some comments in Sec-

tion 5 on the detection of the atmospheric neutrinos in neutrino telescopes and possible signatures of sterile neutrinos in the data sample. We end in Section 6 with discussions and conclusions.

## 2   Neutrino Mixing in Matter with Sterile Neutrinos

Neutrinos would undergo maximum flavor conversion in vacuum when the oscillatory term

$$\sin^2\left(\frac{\Delta m_{ji}^2 L}{4E}\right) = 1 \ , \tag{1}$$

where $L$ and $E$ are the distance travelled by the neutrinos and $\Delta m_{ji}^2 = m_j^2 - m_i^2$. This happens when their energy corresponds to the value

$$
\begin{aligned}
E \ (\text{TeV}) &= 0.81 \times 10^{-3} \left(\Delta m_{ji}^2 \ (\text{eV}^2)\right)\left(L \ (\text{km})\right) , \\
&= 8.1 \times \left(\frac{\Delta m_{ji}^2}{1 \ \text{eV}^2}\right) \times \left(\frac{L}{10{,}000 \ \text{km}}\right) .
\end{aligned}
\tag{2}
$$

Thus we see that if sterile neutrinos are mixed with the active ones with $\Delta m_{ji}^2 \sim \text{eV}^2$, we expect to see maximum flavor conversions for neutrinos with energies in the range of a few TeV, if they are traveling over distances in the range of 10,000 km. High energy atmospheric neutrinos travel distances of this order to reach the neutrino telescopes. They would therefore encounter these flavor oscillations. The amplitude and hence the extent of the oscillations is of course determined by the corresponding mixing angle, which for sterile neutrinos are usually constrained to be extremely small [1]. The combined errors coming from the uncertainties in the predicted high energy atmospheric neutrino fluxes and the experimental uncertainties, could threaten to wash out these oscillations driven by tiny mixing angles.

However, atmospheric neutrino travel through the matter before they reach the detector and this could produce drastic changes in the amplitude of the active-sterile oscillations[2]. In fact, the focal point of this paper is the very large matter effects which the neutrinos pick as they move inside the Earth's matter. In presence of matter the neutrino mass squared matrix changes to [31, 32, 33]

$$M_F^2 = U\mathcal{M}U^\dagger + \mathcal{A} \tag{3}$$

where $U$ is the unitary mixing matrix relating the mass eigenstates to the flavor eigenstates,

$$\mathcal{M} = Diag(m_1^2, m_2^2, m_3^2, m_4^2) \ \text{ or } \ Diag(m_1^2, m_2^2, m_3^2, m_4^2, m_5^2) \ , \tag{4}$$

$$\mathcal{A} = Diag(A_{CC}, 0, 0, A_{NC}) \ \text{ or } \ Diag(A_{CC}, 0, 0, A_{NC}, A_{NC}) \,, \tag{5}$$

---

[1]See [20] for consequences of large active-sterile mixing for ultra high energy neutrino signal in the neutrino telescopes.

[2]Matter effects for very high energy neutrinos due to presence of sterile neutrinos has been discussed before in some form in [28, 29, 30].

for the 3+1 and 3+2 neutrino mass spectrum respectively, where

$$A_{CC} = \pm 2\sqrt{2} G_F \rho N_A Y_e E \,, \tag{6}$$

$$A_{NC} = \pm \sqrt{2} G_F \rho N_A (1 - Y_e) E \,. \tag{7}$$

Here the quantities $A_{CC}$ and $-A_{NC}$ are the matter induced charged current and neutral current potentials respectively, and given in terms of the Fermi constant $G_F$, matter density $\rho$, Avagadro number $N_A$, electron fraction $Y_e$ and energy of the neutrino $E$. The "+" ("−") sign in Eqs. (6) and (7) corresponds to neutrinos (antineutrinos). In the above equations we have re-casted the mass matrix in such a way that the neutral current component $-A_{NC}$, which is negative and which appears for all the three active flavors, is filtered out from the first three diagonal terms and hence it stays back as positive $A_{NC}$ for the sterile state(s), since they do not have any weak interactions. Presence of matter dependent terms in the mass matrix modify the mass squared differences and mixing angles of the neutrinos in matter and these quantities are given respectively as

$$(\Delta m_{ji}^2)^M = \sqrt{(\Delta m_{ji}^2 \cos 2\theta_{ij} - A_M)^2 + (\Delta m_{ji}^2 \sin 2\theta_{ij})^2} \,, \tag{8}$$

$$\sin 2\theta_{ij}^M = \sin 2\theta_{ij} \frac{\Delta m_{ji}^2}{(\Delta m_{ji}^2)^M} \,. \tag{9}$$

In the above we have assumed that only two neutrino states are predominantly involved and depending on which neutrino states these are, $A_M$ could be $A_{CC}$, $A_{NC}$ or $A_{CC} - A_{NC}$. In this approximation the condition for $\nu_e \to \nu_\mu$ or $\nu_e \to \nu_\tau$ resonant transition when $\sin^2 2\theta_{ij}^M = 1$, is given by

$$A_{CC} = \Delta m_{ji}^2 \cos 2\theta_{ij} \,, \tag{10}$$

where $\Delta m_{ji}^2 = m_j^2 - m_i^2$ is the mass squared difference between the two involved states and $\theta_{ij}$ is the corresponding mixing angle. For $\nu_\mu \to \nu_s$ ($\nu_s$ is a sterile state) or $\nu_\tau \to \nu_s$ resonant transition the condition is

$$A_{NC} = -\Delta m_{ji}^2 \cos 2\theta_{ij} \,, \tag{11}$$

while for $\nu_e \to \nu_s$ the resonance condition is

$$A_{CC} - A_{NC} = \Delta m_{ji}^2 \cos 2\theta_{ij} \,. \tag{12}$$

Since $A_{CC}$ and $A_{NC}$ are both positive for neutrinos and both negative for antineutrinos, and since $Y_e \simeq 0.5$ giving $A_{CC} \simeq 2A_{NC}$ for Earth matter, this resonance condition (12) is satisfied for neutrinos when $\Delta m_{ji}^2 > 0$ and for antineutrinos when $\Delta m_{ji}^2 < 0$. On the other hand, the $\nu_\mu \to \nu_s$ or $\nu_\tau \to \nu_s$ resonance condition will be satisfied for neutrinos (antineutrinos) when $\Delta m_{ji}^2 < 0$ ($\Delta m_{ji}^2 > 0$). The $\nu_e \to \nu_\mu$ or $\nu_e \to \nu_\tau$ resonance will happen in the neutrino (antineutrino) channel when $\Delta m_{ji}^2 > 0$ ($\Delta m_{ji}^2 < 0$). Since we have both neutrinos and antineutrinos coming

from the atmosphere, we could have resonance in either the neutrino or the antineutrino channel for a given $sgn(\Delta m_{ji}^2)$, if any of the above conditions are satisfied.

All results presented in this paper are generated by exactly solving the full set of evolution equations for the neutrinos travelling through Earth matter parameterized by the PREM density profile [34]. However, just for simplicity let us for the moment assume that the neutrino travel through constant density matter inside the Earth. Assuming that $Y_e = 0.5$, the very high energy atmospheric neutrinos travelling through the Earth would pick matter potential of

$$A_{CC} = 1.907 \; (\text{eV}^2) \times \left( \frac{\rho}{5.0 \text{ gm/cc}} \right) \left( \frac{E}{5.0 \text{ TeV}} \right) , \tag{13}$$

$$A_{NC} = 0.954 \; (\text{eV}^2) \times \left( \frac{\rho}{5.0 \text{ gm/cc}} \right) \left( \frac{E}{5.0 \text{ TeV}} \right) , \tag{14}$$

$$A_{CC} - A_{NC} = 0.953 \; (\text{eV}^2) \times \left( \frac{\rho}{5.0 \text{ gm/cc}} \right) \left( \frac{E}{5.0 \text{ TeV}} \right) . \tag{15}$$

Therefore, we see that the resonance conditions given by Eqs. (10), (11), and (12) can be easily satisfied for $\Delta m_{4i}^2$ and $\Delta m_{5i}^2$ relevant for LSND and MiniBooNE, where $i = 1, 2, 3$. We could also turn around these equations to give us the resonance energy as

$$E_{res}^{\nu_e \to \nu_a}(\text{TeV}) = \frac{\Delta m_{4i}^2 \cos 2\theta_{i4}}{0.076 \times \left( \rho(\text{gm/cc}) \right)} , \tag{16}$$

$$E_{res}^{\nu_a \to \nu_s}(\text{TeV}) = \frac{\Delta m_{4i}^2 \cos 2\theta_{i4}}{0.038 \times \left( \rho(\text{gm/cc}) \right)} , \tag{17}$$

$$E_{res}^{\nu_e \to \nu_s}(\text{TeV}) = \frac{\Delta m_{4i}^2 \cos 2\theta_{i4}}{0.038 \times \left( \rho(\text{gm/cc}) \right)} , \tag{18}$$

where $a$ in the above equations refer to either the $\mu$ or $\tau$ flavor. For the $\Delta m_{5i}^2$ case we have the same relations with $\Delta m_{4i}^2$ replaced by $\Delta m_{5i}^2$. Therefore, for neutrinos crossing the core (mantle only) of the Earth for which the average matter density is $\sim 8$ gm/cc ($\sim 5$ gm/cc), we expect resonance for $E \sim 3$ GeV ($\sim 5$ GeV) if we assume $\Delta m_{4i}^2$ and $\Delta m_{5i}^2$ to be about 1 eV$^2$. We note that the energy at which we expect to see $\nu_e \to \nu_s$ resonance is the same as the one where we are expecting to get $\nu_a \to \nu_s$ resonance. On the other hand the energy at which we will get $\nu_e \to \nu_a$ resonance will be lower by a factor of about 2. We get similar expressions also for $\Delta m_{5i}^2$ induced resonances. Note that even though we have given the discussion for the $\Delta m^2 \sim$ eV$^2$ driven $\nu_e \to \nu_a$ resonance for completeness, this resonance never happens in the 3+1 or 3+2 scenario inside the Earth since the $\Delta m^2$ involved between the $\nu_e$ and $\nu_a$ states are the ones needed to explain the solar and atmospheric neutrino data and hence definitely not of the eV$^2$ scale that we are interested in. The mass eigenstates $\nu_4$ and $\nu_5$ are predominantly composed of the sterile components and hence the $\Delta m_{41}^2$ and $\Delta m_{51}^2$ mass squared difference drive the active-sterile resonances only. We remind the reader of the well known fact that when the resonance condition is satisfied, the corresponding mixing angle, even if it was very small in vacuum, becomes maximal in matter. Thus the amplitude factor in the oscillation probability also becomes maximal.

The oscillation probabilities in matter are given by the most general expression

$$
P_{\beta\gamma}(L) = \quad \delta_{\beta\gamma} \quad -4\sum_{j>1} \Re\left( U_{\beta i}^M U_{\gamma i}^{M\star} U_{\beta j}^{M\star} U_{\gamma j}^M \right) \sin^2 \frac{(\Delta m_{ij}^2)^M L}{4E}
$$

$$
+2\sum_{j>1} \Im\left( U_{\beta i}^M U_{\gamma i}^{M\star} U_{\beta j}^{M\star} U_{\gamma j}^M \right) \sin \frac{(\Delta m_{ij}^2)^M L}{2E}, \tag{19}
$$

where $(\Delta m_{ij}^2)^M$ and $U^M$ are respectively the modified mass squared difference and mixing matrix in matter. The mixing matrix is parameterized in terms of the mixing angles (in matter). For the 3+1 case we will have 6 mixing angles, while for the 3+2 scenario $U^M$ is given in terms of 10 angles. In fact, the most general form of the mixing matrix $U^M$ is complex and this CP dependence is probed through the last term in Eq. (19). But for simplicity, we will put all CP violating phases in $U^M$ to zero and hence the last term in Eq. (19) goes to zero. Also for TeV energy neutrinos, the oscillations induced by $\Delta m_{21}^2$ and $\Delta m_{31}^2$ are negligible and we will get contributions from mainly the oscillatory terms corresponding to the mass squared difference associated with the sterile states. We reiterate that each term in the oscillation probability contains a product of the mass squared dependent oscillatory term and the mixing angle dependent term. Therefore, to achieve maximal oscillations in Earth matter, it is not enough to satisfy only the condition of resonance where the mixing angle becomes maximal. We should should simultaneously have the peak of the oscillatory term [35]. Thus one obtains maximal oscillations when the condition

$$
\rho L \text{ (km gm/cc)} = \frac{33.55 \times 10^3}{\tan 2\theta_{ij}} \ , \tag{20}
$$

is satisfied. We have assumed a constant density for the Earth matter, $L$ is the baseline where maximal oscillations happen and $\rho$ is the corresponding average density. We will discuss this issue in greater details in the following section.

# 3 Neutrino Oscillations with 3+1 Mass Spectrum

We start by showing results for the case where there is only one extra sterile neutrino. For 4 neutrinos we have 3 mass squared differences. For $\Delta m_{21}^2$ and $\Delta m_{31}^2$ we take the current best-fit values coming from global neutrino oscillation data, while for $\Delta m_{41}^2$ we take different values in the eV$^2$ range. For the mixing matrix we choose the following convention:

$$
U = R(\theta_{34})R(\theta_{24})R(\theta_{23})R(\theta_{14})R(\theta_{13})R(\theta_{12}) \ , \tag{21}
$$

where $R(\theta_{ij})$ are the rotation matrices and $\theta_{ij}$ the mixing angle. In general for the 3+1 scenario there are 3 CP violating Dirac phases. However as mentioned before, we have put all phases to zero in Eq. (21) for simplicity. The expressions for the oscillation probabilities relevant for atmospheric neutrinos then take the simple form

$$
P_{\mu\mu} \ \simeq \ 1 - \left( \sin^2 \theta_{24}^M \sin^2 2\theta_{14}^M + \cos^2 \theta_{14}^M \sin^2 2\theta_{24}^M \right) \sin^2 \left[ \frac{(\Delta m_{41}^2)^M L}{4E} \right], \tag{22}
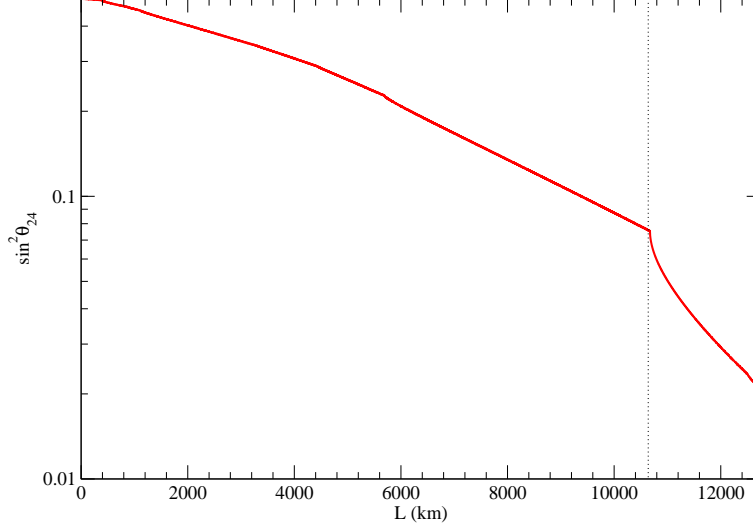$$

Figure 1: Values of $\sin^2 \theta_{24}$ at which we have maximal oscillations as a function of the distance $L$ travelled inside Earth. We have assumed $\sin^2 \theta_{14} = 0$ and $\sin^2 \theta_{34} = 0$ and the 3+1 mass spectrum. The dashed line shows the boundary between the mantle and core of the Earth.

$$P_{\mu e} \simeq \sin^2 2\theta_{14}^M \sin^2 \theta_{24}^M \sin^2 \left[ \frac{(\Delta m_{41}^2)^M L}{4E} \right], \tag{23}$$

$$P_{\mu \tau} \simeq \cos^2 \theta_{14}^M \sin^2 2\theta_{24}^M \sin^2 \theta_{34}^M \sin^2 \left[ \frac{(\Delta m_{41}^2)^M L}{4E} \right], \tag{24}$$

$$P_{\mu s} \simeq \cos^2 \theta_{14}^M \sin^2 2\theta_{24}^M \cos^2 \theta_{34}^M \sin^2 \left[ \frac{(\Delta m_{41}^2)^M L}{4E} \right], \tag{25}$$

$$P_{ee} \simeq 1 - \sin^2 2\theta_{14}^M \sin^2 \left[ \frac{(\Delta m_{41}^2)^M L}{4E} \right], \tag{26}$$

$$P_{e \tau} \simeq \sin^2 2\theta_{14}^M \cos^2 \theta_{24}^M \sin^2 \theta_{34}^M \sin^2 \left[ \frac{(\Delta m_{41}^2)^M L}{4E} \right]. \tag{27}$$

We note that the probabilities depend only on the 3 extra mixing angles $\theta_{14}$, $\theta_{24}$ and $\theta_{34}$. In particular, $P_{\mu e}$ and $P_{\mu \mu}$ depend explictly on $\theta_{14}$ and $\theta_{24}$ and it seems that it is *apparently* independent of $\theta_{34}$. We will see that this is not the case always and there is an implicit $\theta_{34}$ dependence due to matter effects.

The mixing angle $\theta_{14}$ affects strongly the $P_{ee}$ channel. But in this section, we keep fixed $\theta_{14} = 0$ for simplicity and concentrate on the oscillation channels affecting the muon type (anti)neutrino. We will probe the impact of $\theta_{14}$ in the more realistic 3+2 scenario in next section. We first present results where the mixing angle $\theta_{34}$ is also fixed at 0 and only $\theta_{24}$ is the non-zero sterile mixing angle. Finally we present results where both $\theta_{24}$ and $\theta_{34}$ are non-zero.
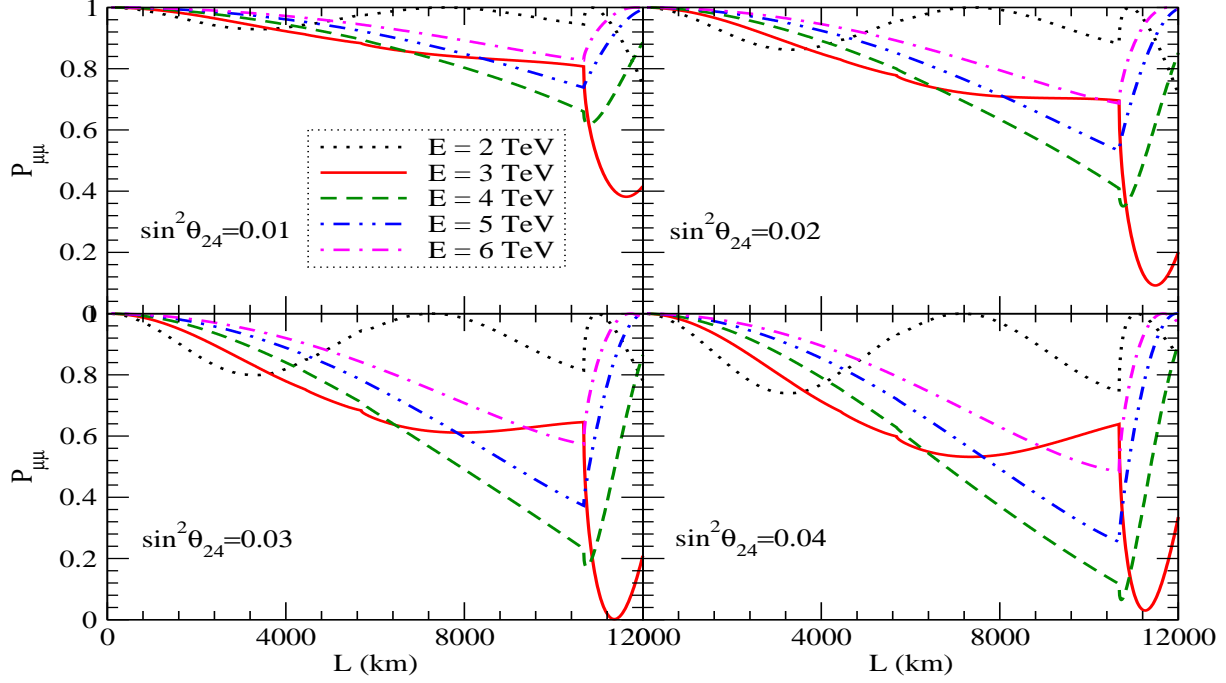
8

Figure 2: The survival probability $P_{\mu\mu}$ as a function of $L$ using the PREM profile for the Earth density. The different line types correspond to different fixed values of $E$ and each panel shows the results for different fixed values of $\sin^2\theta_{24}$ given in the panels. We have assumed the 3+1 mass spectrum and taken $|\Delta m_{41}^2| = 1$ eV$^2$, $\sin^2\theta_{14} = 0$ and $\sin^2\theta_{34} = 0$. The probability corresponds to neutrinos for $\Delta m_{41}^2 < 0$ and to antineutrinos for $\Delta m_{41}^2 > 0$.

## 3.1 Oscillation Probabilities in 3+1 when $\theta_{14} = 0$ and $\theta_{34} = 0$

For both $\theta_{14} = 0$ and $\theta_{34} = 0$, the probabilities assume very simple forms

$$P_{\mu\mu} \simeq 1 - \sin^2 2\theta_{24}^M \sin^2\left[\frac{(\Delta m_{41}^2)^M L}{4E}\right], \tag{28}$$

$$P_{\mu s} \simeq \sin^2 2\theta_{24}^M \sin^2\left[\frac{(\Delta m_{41}^2)^M L}{4E}\right], \tag{29}$$

$$P_{\mu e} \simeq 0, \quad P_{\mu\tau} \simeq 0, \quad P_{e\tau} \simeq 0, \quad P_{ee} \simeq 1. \tag{30}$$

This is therefore a case of simple two-generation $\nu_\mu - \nu_s$ oscillations. The mixing angle and mass squared difference in matter are given as

$$\sin 2\theta_{24}^M = \sin 2\theta_{24} \frac{\Delta m_{41}^2}{(\Delta m_{41}^2)^M}, \tag{31}$$

$$(\Delta m_{41}^2)^M = \sqrt{(\Delta m_{41}^2 \cos 2\theta_{24} \pm \sqrt{2} G_F N_A \rho Y_e E)^2 + (\Delta m_{41}^2 \sin 2\theta_{24})^2}, \tag{32}$$
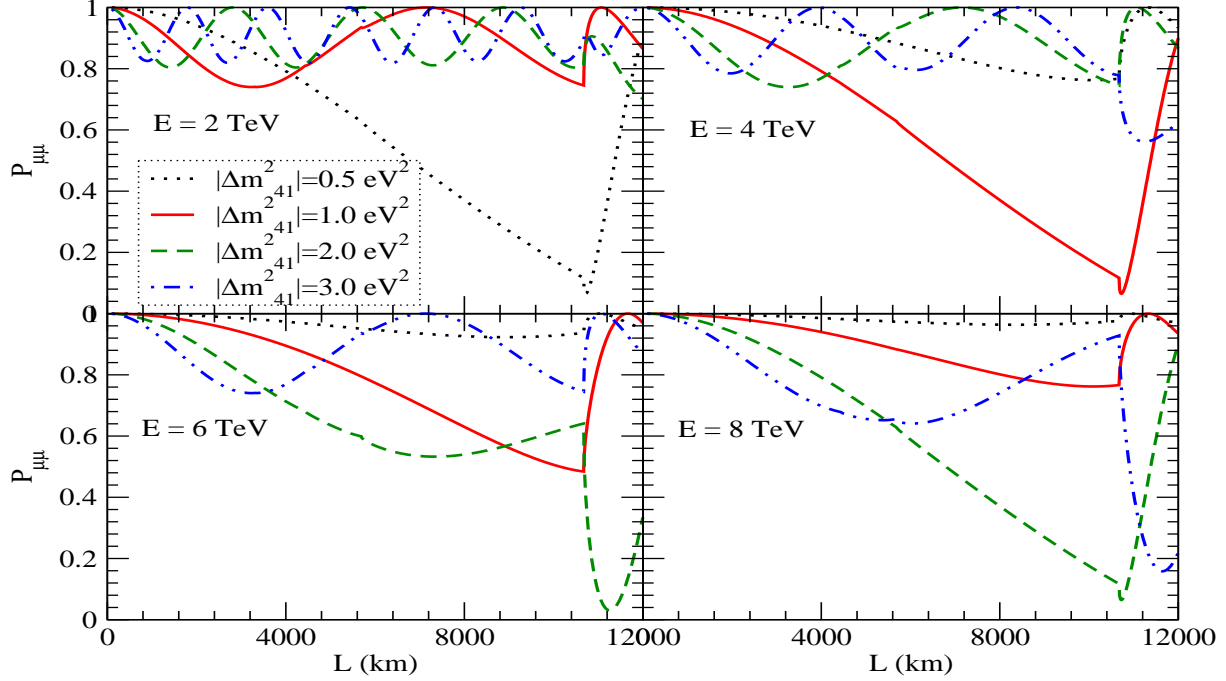
9

Figure 3: The survival probability $P_{\mu\mu}$ as a function of $L$ using the PREM profile for the Earth density. The different line types correspond to different fixed values of $|\Delta m_{41}^2|$ and each panel shows the results for different fixed values of $E$ given in the panels. We have assumed the 3+1 mass spectrum and taken $\sin^2\theta_{24} = 0.04$ eV$^2$, $\sin^2\theta_{14} = 0$ and $\sin^2\theta_{34} = 0$. The probability corresponds to neutrinos for $\Delta m_{41}^2 < 0$ and to antineutrinos for $\Delta m_{41}^2 > 0$.

where the $+$ sign is for neutrino and $-$ sign for the antineutrinos. Note that we have used $\Delta m_{41}^2 \simeq \Delta m_{42}^2$. As discussed before, we have resonant matter effects and $\sin^2 2\theta_{24}^M = 1$ in the neutrino (antineutrino) channel when $\Delta m_{41}^2 < 0$ ($\Delta m_{41}^2 > 0$). However, the condition of resonance does not necessarily give the largest possible oscillations. The condition for maximal oscillation is achieved when both $\sin^2 2\theta_{24}^M = 1$ and $\sin^2[(\Delta m_{41}^2)^M L/4E] = 1$ simultaneously [35] and is given by Eq. (20). It can be inverted to give the value of $\theta_{24}$ which would give maximal oscillations at a given baseline:

$$\tan 2\theta_{24} = \frac{32.55 \times 10^3}{\rho L \text{ (km gm/cc)}} \ . \tag{33}$$

For values of $\theta_{24}$ either less or greater than the value corresponding to that obtained from Eq. (33), the oscillations are less [36]. We show in Fig. 1 the value of $\sin^2\theta_{24}$ for which we can have maximal oscillations, as a function of distance $L$ travelled inside Earth. For $\rho$ we have used the average density along the neutrino trajectory given by the PREM profile. The dashed line shows the mantle-core boundary of Earth and we can see that for the more plausible values of $\sin^2\theta_{24} \lesssim 0.07$ the condition for maximal oscillations are always met inside the Earth's core. In

10

particular, for the longest possible trajectory where $L = 2 \times R_E$, $R_E$ being the Earth's radius, we note that maximal oscillations will happen if $\sin^2 \theta_{24} = 0.02$.

Fig. 2 shows the survival probability $P_{\mu\mu}$ as a function of the distance travelled inside the Earth. For this plot we use the full PREM density profile for the Earth and solve the four neutrino differential equation in matter. The different line types correspond to different fixed values of $E$ and each panel shows the results for different fixed values of $\sin^2 \theta_{24}$ given in the panels. The probability shown would correspond to that for neutrinos if $\Delta m_{41}^2 < 0$ and to antineutrinos if $\Delta m_{41}^2 > 0$. We note from the figure that for most neutrino energies above $E \gtrsim 2$ TeV, there are sizeable matter effects inside Earth and the survival probability generally decreases with $L$ in the mantle. Inside the core it falls first, followed by a rise. However, we can see that for reasonable $L$ binning of the high energy atmospheric neutrino data in neutrino telescopes, it should be possible to see zenith angle dependent fall in $P_{\mu\mu}$. Even for very small values of $\sin^2 \theta_{24}$ like 0.01, we can see that $P_{\mu\mu}$ could fall to up to 0.6, and this should be observable in the detector.

Fig. 3 is similar to Fig. 2, except that here we show the probability at a fixed value of $\sin^2 \theta_{24}$, but different choices of $|\Delta m_{41}^2|$ and $E$. All plots are for $\sin^2 \theta_{24} = 0.04$ and each panel for a fixed $E$, shown in the figure. The different line types correspond to different $|\Delta m_{41}^2|$. As before, the probability corresponds to neutrinos for $\Delta m_{41}^2 < 0$ and to antineutrinos for $\Delta m_{41}^2 > 0$. This figure tells us how different values of $|\Delta m_{41}^2|$ can be distinguished from the high energy atmospheric neutrino data at the neutrino telescopes. We can see that binning in either or both $E$ and $L$ would help in distinguishing between the different possible $|\Delta m_{41}^2|$ values.

## 3.2 Oscillation Probabilities in 3+1 when $\theta_{14} = 0$ and $\theta_{34} \neq 0$

If we allow $\sin^2 \theta_{34} \neq 0$ but still keep $\theta_{14} = 0$, the probabilities are given as

$$P_{\mu\mu} \simeq 1 - \sin^2 2\theta_{24}^M \sin^2 \left[ \frac{(\Delta m_{41}^2)^M L}{4E} \right], \tag{34}$$

$$P_{\mu\tau} \simeq \sin^2 2\theta_{24}^M \sin^2 \theta_{34}^M \sin^2 \left[ \frac{(\Delta m_{41}^2)^M L}{4E} \right], \tag{35}$$

$$P_{\mu s} \simeq \sin^2 2\theta_{24}^M \cos^2 \theta_{34}^M \sin^2 \left[ \frac{(\Delta m_{41}^2)^M L}{4E} \right], \tag{36}$$

$$P_{\mu e} \simeq 0, \quad P_{e\tau} \simeq 0, \quad P_{ee} \simeq 1. \tag{37}$$

Fig. 4 shows the neutrino oscillation probabilities assuming inverted mass ordering, taking $\Delta m_{41}^2 = -1$ eV$^2$. The $\nu_\mu \to \nu_\mu$, $\nu_\mu \to \nu_\tau$ and $\nu_\mu \to \nu_s$ probabilities are shown in the upper left hand panel, upper right hand panel and lower right hand panel, respectively. For $\sin^2 \theta_{14} = 0$, the probabilities $P_{\mu e} \simeq 0$, $P_{e\tau} \simeq 0$ and $P_{ee} \simeq 1$ and hence we do not show them. The solid black (dark) line is for neutrinos in matter and the solid cyan (light) line is for antineutrinos in matter, while the thin black dashed line shows the probabilities in vacuum for comparison. We stress that even though we have denoted the probabilities as $\nu_\mu \to \nu_\mu$ etc. in the figure, its understood that we are using them to denote the probability for both the neutrino as well as the antineutrino channels. We have kept $\sin^2 \theta_{24} = \sin^2 \theta_{34} = 0.04$ in this figure. The corresponding plots with the normal mass ordering is shown in Fig. 5. The neutrinos (antineutrinos) undergo maximal oscillations around
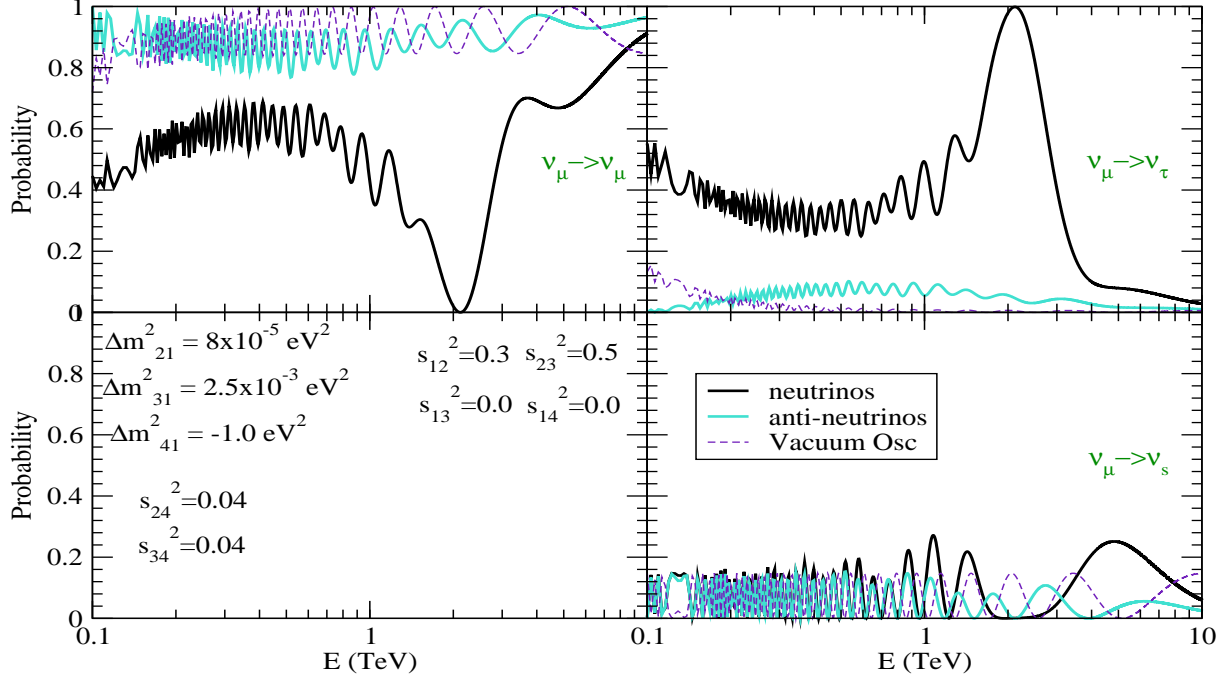
Figure 4: The $\nu_\mu \to \nu_\mu$ (upper left hand panel), $\nu_\mu \to \nu_\tau$ (upper right hand panel) and $\nu_\mu \to \nu_s$ (lower right hand panel) oscillation probabilities, as a function of the neutrino energy $E$ for the 3+1 mass spectrum, when the neutrinos travel a distance $L = 2R_e$, where $R_e$ is the radius of the Earth. The black (dark) solid lines show the probabilities for neutrinos while the cyan (light) solid lines show the probabilities for antineutrinos. The dashed lines give the probabilities if matter effects were not taken into account and one had oscillations in vacuum. The values of the oscillation parameters taken for this figure is shown in the lower left hand panel. In particular this plot is for $\Delta m_{41}^2 = 1$ eV$^2$. Probabilities in matter have been obtained using the PREM profile.

$E = 2$ TeV when $\Delta m_{41}^2 = -1$ eV$^2$ ($\Delta m_{41}^2 = +1$ eV$^2$). At lower values of $E$, where very large matter effects in $\Delta m_{41}^2$ oscillations have still not set in, we note a marked difference between the oscillations pattern of neutrinos and antineutrinos and between the cases where $\Delta m_{41}^2 < 0$ and $\Delta m_{41}^2 > 0$. The oscillations for lower $E$ are dependent on $\Delta m_{31}^2$ as well and the difference between the oscillation mentioned above is due to both $\Delta m_{31}^2$ and $\Delta m_{41}^2$ dependent terms. Note that in both cases we have kept $\Delta m_{31}^2 > 0$. The most important thing to note from this figure is that around the point where we have maximal matter effects, $P_{\mu\mu} \simeq 0$, $P_{\mu\tau} \simeq 1$ and $P_{\mu s} \simeq 0$ for the neutrino (antineutrino) channel for $\Delta m_{41}^2 < 0$ ($\Delta m_{41}^2 > 0$). Such large oscillations should not be difficult to observe in the very high atmospheric neutrino data in neutrino telescopes.

In the previous subsection where we had put $\theta_{34} = 0$, we had argued that for $L = 2R_e$, where $R_e$ is the Earth's radius, maximal oscillations of $\nu_\mu$ would occur around $\sin^2\theta_{24} \simeq 0.02$. For $\sin^2\theta_{24} = 0.04$ we should therefore expect lesser oscillations. We had drawn these conclusions using average constant matter density approximation for the Earth. For the PREM profile which
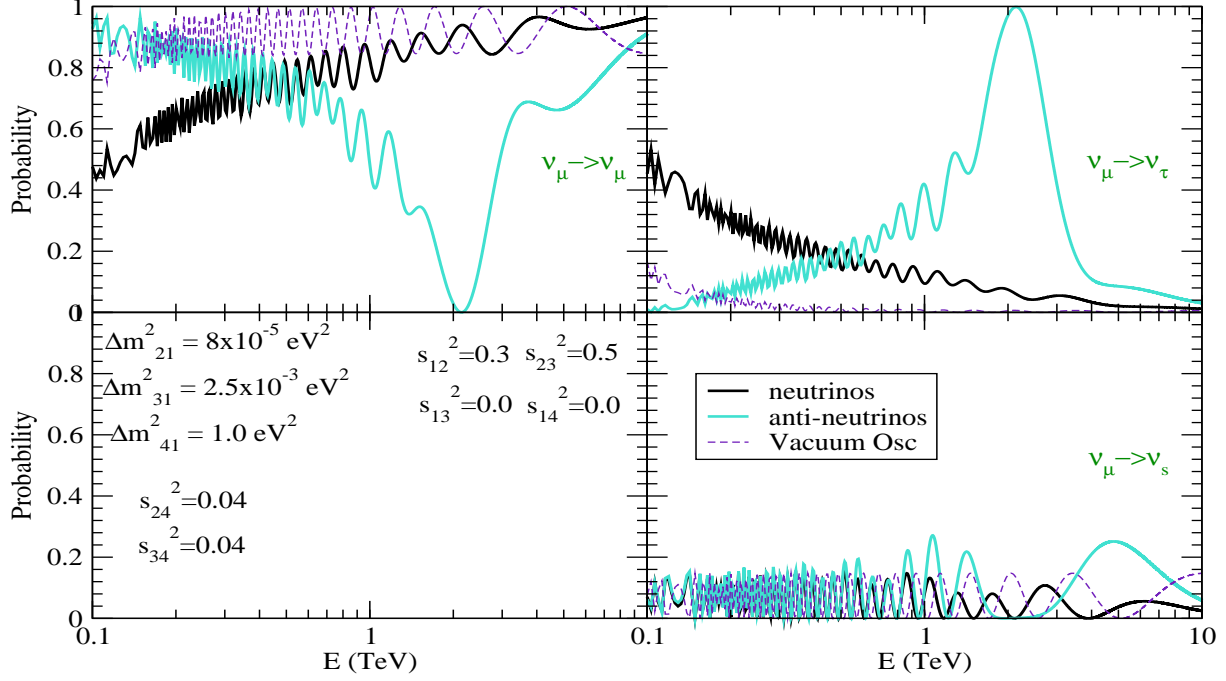
Figure 5: Same as Fig. 4 but for $\Delta m_{41}^2 = +1$ eV$^2$.

corresponds to varying matter density for the Earth, this scenario holds, albeit approximately. In Figs. 4 and 5 we can see that we get maximal oscillations even for $\sin^2 \theta_{24} = 0.04$ as long as $\sin^2 \theta_{34} = 0.04$. Another important aspect we note from the figures is that $P_{\mu\tau} \simeq 1$ and $P_{\mu s} \simeq 0$ when we have maximal oscillations of $\nu_\mu$. This is in stark contrast to the case where $\sin^2 \theta_{34} = 0$, for which we had $P_{\mu\tau} \simeq 0$ and $P_{\mu s} \simeq 1$ (cf. Eqs. (29) and (30)). The main reason for this complete reversal of scenario is that when $\sin^2 \theta_{24} \neq 0$ and $\sin^2 \theta_{34} = 0$, $\sin^2 \theta_{24}^M$ is enhanced in matter for neutrinos (antineutrinos) when $\Delta m_{41}^2 < 0$ ($\Delta m_{41}^2 > 0$) while $\sin^2 \theta_{34}^M$ remains zero. Therefore, $P_{\mu\tau}$ is always zero and we have simple two-generation matter enhanced $\nu_\mu \rightarrow \nu_s$ oscillations. However, when $\sin^2 \theta_{34} \neq 0$, both $\sin^2 \theta_{24}$ and $\sin^2 \theta_{34}$ are enhanced in matter for neutrinos (antineutrinos) when $\Delta m_{41}^2 < 0$ ($\Delta m_{41}^2 > 0$). This is a genuine three-generation oscillation case in which if $\sin^2 \theta_{34} = \sin^2 \theta_{24}$, the $\nu_\mu$ and $\nu_\tau$ states evolve identically in matter and resonate with the sterile state at almost the same energy.

To further illustrate this point we present Fig. 6, where we compare the probabilities corresponding to $L = 2R_e$, for the cases where $\sin^2 \theta_{34} = 0$ with those where $\sin^2 \theta_{34} \neq 0$. We show $P_{\mu\mu}$, $P_{\mu\tau}$ and $P_{\mu s}$ for $\sin^2 \theta_{24} = 0.02$, $\sin^2 \theta_{34} = 0.00$ (black solid lines), $\sin^2 \theta_{24} = 0.02$, $\sin^2 \theta_{34} = 0.02$ (red dot-dashed lines), $\sin^2 \theta_{24} = 0.04$, $\sin^2 \theta_{34} = 0.00$ (green dotted lines), and $\sin^2 \theta_{24} = 0.04$, $\sin^2 \theta_{34} = 0.02$ (blue dashed lines). We reconfirm that for $\sin^2 \theta_{24} = 0.02$ and $\sin^2 \theta_{34} = 0$ we have $P_{\mu\mu} \simeq 0$ and $P_{\mu s} \simeq 1$. For $\sin^2 \theta_{24} = 0.04$ and $\sin^2 \theta_{34} = 0$, we still have two-generation $\nu_\mu \rightarrow \nu_s$ oscillations with $P_{\mu\tau} = 0$, but now since we have shifted from the most optimal $\sin^2 \theta_{24}$ value for this baseline, $P_{\mu\mu}$ increases and $P_{\mu s}$ decreases compared to the case where $\sin^2 \theta_{24} = 0.02$. Once we put
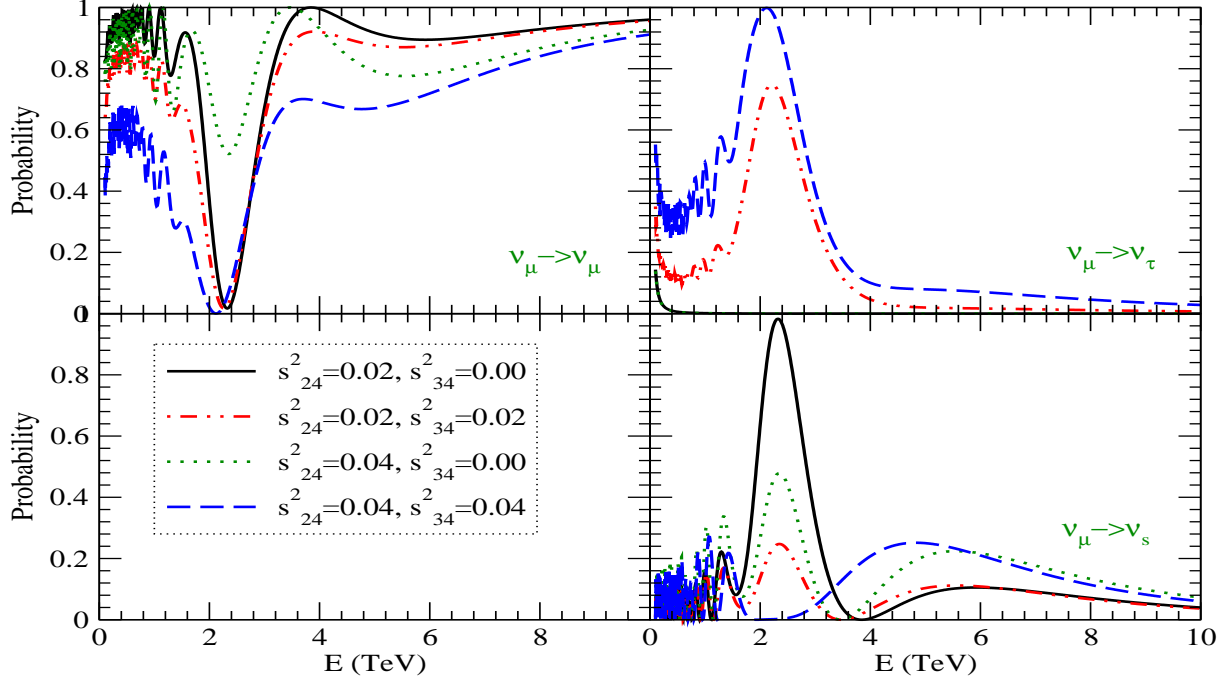
13

Figure 6: The $\nu_\mu \to \nu_\mu$ (upper left hand panel), $\nu_\mu \to \nu_\tau$ (upper right hand panel) and $\nu_\mu \to \nu_s$ (lower right hand panel) oscillation probabilities, as a function of the neutrino energy $E$, when the neutrinos travel a distance $L = 2R_e$, where $R_e$ is the radius of the Earth. Different line types correspond to different combinations of $\sin^2 \theta_{24}$ and $\sin^2 \theta_{34}$ and $\Delta m_{41}^2 = -1$ eV$^2$.

$\sin^2 \theta_{34} = \sin^2 \theta_{24}$, we get $P_{\mu\mu} \simeq 0$ for both $\sin^2 \theta_{24} = 0.02$ and $\sin^2 \theta_{24} = 0.04$. However, non-zero $\sin^2 \theta_{34}$ brings a huge change in $P_{\mu\tau}$ which becomes non-zero and large and for $\sin^2 \theta_{34} = 0.04$, it is in fact very close to 1. Likewise, $P_{\mu s}$ changes substantially due to $\sin^2 \theta_{34}$.

In order to quantify our discussion on the impact of $\sin^2 \theta_{34}$ on the evolution of the neutrino states inside Earth, we show in Fig. 7 the mixing angles in matter as a function of $E$. Since its not possible to show the evolution of the mixing angles for the full PREM profile, we show a snapshot for a density of $\rho = 8.44$ gm/cc, which is the average density encountered by a neutrino moving along the diameter of the Earth. The green dot-dashed line shows $\sin^2 \theta_{24}^M$ when $\sin^2 \theta_{24} = 0.04$ and $\sin^2 \theta_{34} = 0$ in vacuum. We see that the mixing angle increases with energy and hence matter effects. At the resonance energy we get $\sin^2 2\theta_{24}^M = 1$ and beyond that $\sin^2 \theta_{24}^M$ keeps increasing to 1 and $\sin^2 2\theta_{24}^M$ decreases. The evolution of $\sin^2 \theta_{24}^M$ when $\sin^2 \theta_{24} = 0.04$ and $\sin^2 \theta_{34} = 0.04$ is shown by the black dotted line. This case is very different from the earlier described case. Here $\sin^2 \theta_{24}^M$ remains more or less constant beyond the resonance and hence $\sin^2 2\theta_{24}^M$ assumes some large constant value and does not decrease like before. Note that the reason we were getting lesser oscillations in the $P_{\mu\mu}$ channel for $\sin^2 \theta_{24} = 0.04$ (and $\sin^2 \theta_{34} = 0$) was because the resonance energy here was not matching exactly with the energy as which the oscillatory term peaks. But for $\sin^2 \theta_{24} = 0.04$ and $\sin^2 \theta_{34} = 0.04$ since $\sin^2 2\theta_{24}^M$ has a large value from energies beyond
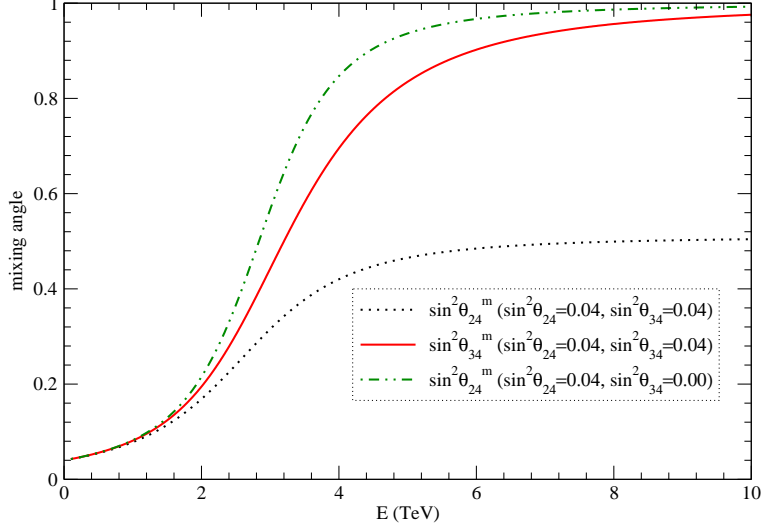
14

Figure 7: The mixing angles in matter as a function of the neutrino energy. The dotted and solid lines show $\sin^2 \theta_{24}^M$ and $\sin^2 \theta_{34}^M$ when their values in vacuum are $\sin^2 \theta_{24} = 0.04$ and $\sin^2 \theta_{34} = 0.04$. The dotted-dashed lines show $\sin^2 \theta_{24}^M$ when the values in vacuum are $\sin^2 \theta_{24} = 0.04$ and $\sin^2 \theta_{34} = 0.00$.

the resonance, the problem of fine tuning the resonance energy and oscillations peak energy is drastically reduced and we can have $P_{\mu\mu} \simeq 0$ more easily. The reason for the change in behavior of $P_{\mu\tau}$ and $P_{\mu s}$ with $\sin^2 \theta_{34} \neq 0$ can also be seen from Fig. 7. The red solid line shows the angle $\sin^2 \theta_{34}^M$ and we see that this keeps increasing and goes to 1 for $E$ greater than the resonance energy. Since $P_{\mu\tau}$ is proportional to $\sin^2 \theta_{34}^M$ and $P_{\mu s}$ to $\cos^2 \theta_{34}^M$, $P_{\mu\tau}$ increases while $P_{\mu s}$ decreases as $\sin^2 \theta_{34}^M$ increases.

# 4   Neutrino Oscillations with 3+2 Mass Spectrum

The 3+1 neutrino mass spectrum, though simpler for the understanding of the resonant oscillation picture, stands disfavored comprehensively once the latest MiniBooNE results are included into the analysis along with results from all other neutrino oscillation experiments. However, the 3+2 scheme, with two extra sterile neutrinos, provides a very reasonable description of the world neutrino data, including MiniBooNE. In this section we look at the predicted neutrino and antineutrino oscillation probabilities at neutrino telescopes for the 3+2 neutrino mass scheme. The expression for the oscillation probabilities in the 3+2 scheme are as follows:

$$
\begin{aligned}
P_{\alpha\alpha} = 1 \ -\ & 4|U_{\alpha 4}^M|^2\left(1 - |U_{\alpha 4}^M|^2\right)\sin^2\left(\frac{(\Delta m_{41}^2)^M L}{4E}\right) - 4|U_{\alpha 5}^M|^2\left(1 - |U_{\alpha 5}^M|^2\right)\sin^2\left(\frac{(\Delta m_{51}^2)^M L}{4E}\right) \\
+\ & 8|U_{\alpha 4}^M|^2|U_{\alpha 5}^M|^2 \sin\left(\frac{(\Delta m_{41}^2)^M L}{4E}\right)\sin\left(\frac{(\Delta m_{51}^2)^M L}{4E}\right)\sin\left(\frac{(\Delta m_{54}^2)^M L}{4E}\right),
\end{aligned}
\tag{38}
$$

15

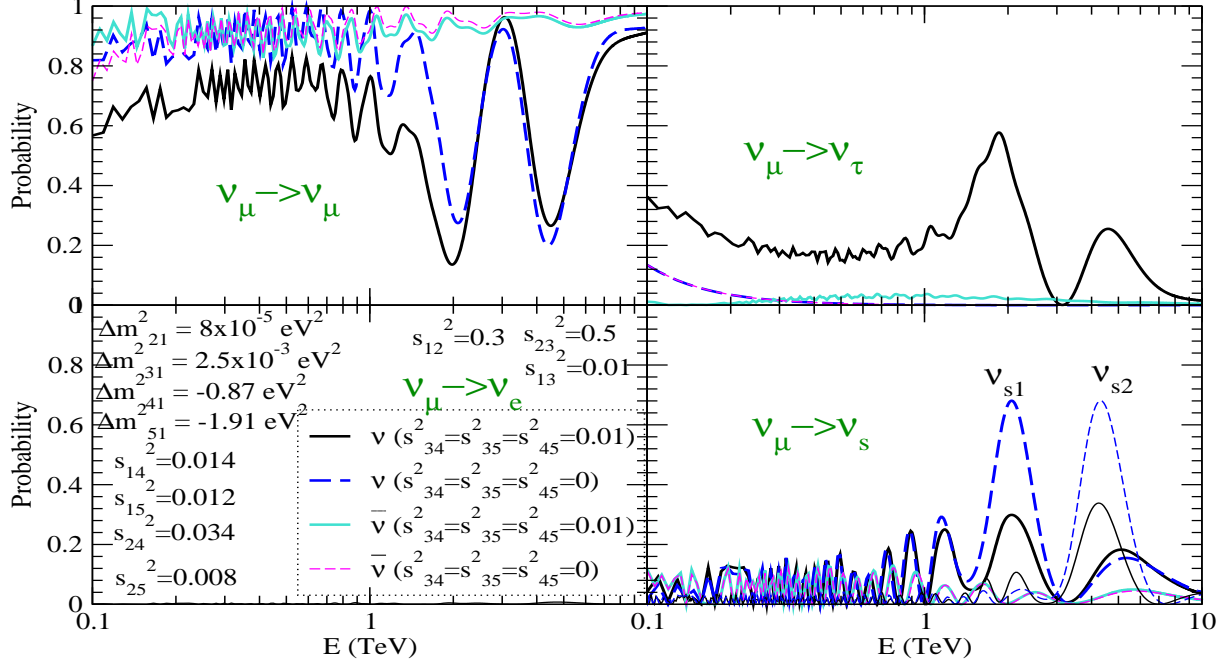Figure 8: The $\nu_\mu \to \nu_\mu$ (upper left hand panel), $\nu_\mu \to \nu_\tau$ (upper right hand panel), $\nu_\mu \to \nu_e$ (lower left hand panel), and $\nu_e \to \nu_{s1}$ and $\nu_e \to \nu_{s2}$ (lower right hand panel) oscillation probabilities, as a function of the neutrino energy $E$ for the 3+2 mass spectrum, when the neutrinos travel a distance $L = 2R_e$, where $R_e$ is the radius of the Earth. The solid black and dashed blue lines show the probabilities for neutrinos while the solid cyan and thin dashed magenta lines are for the antineutrinos. The solid black and solid cyan lines are drawn for $\sin^2\theta_{34} = \sin^2\theta_{35} = \sin^2\theta_{45} = 0.01$, while the dashed blue and dashed magenta lines are for $\sin^2\theta_{34} = \sin^2\theta_{35} = \sin^2\theta_{45} = 0.0$. The values of the other oscillation parameters are shown in the figure and we have taken $\Delta m^2_{41} = -0.87$ eV$^2$ and $\Delta m^2_{51} = -1.91$ eV$^2$. For $\nu_\mu \to \nu_s$, we show the $\nu_\mu \to \nu_{s1}$ by thick line and $\nu_\mu \to \nu_{s2}$ by thin line.

$$P_{\alpha\beta} = \quad 4|U^M_{\alpha 4}|^2|U^M_{\beta 4}|^2 \sin^2\left(\frac{(\Delta m^2_{41})^M L}{4E}\right) + 4|U^M_{\alpha 5}|^2|U^M_{\beta 5}|^2 \sin^2\left(\frac{(\Delta m^2_{51})^M L}{4E}\right) \cdot$$

$$+ \quad 8|U^M_{\alpha 4}U^{M*}_{\beta 4}U^{M*}_{\alpha 5}U^M_{\beta 5}|\sin\left(\frac{(\Delta m^2_{41})^M L}{4E}\right)\sin\left(\frac{(\Delta m^2_{51})^M L}{4E}\right)\cos\left(\frac{(\Delta m^2_{54})^M L}{4E}\right) \quad (39)$$

Note that if we had taken into account CP violating phases in $U$, the argument in the cosine of the last term in Eq. (39) would be $(\Delta m^2_{54})^M L/4E - \delta_{\alpha\beta}$ where $\delta_{\alpha\beta} = Arg(U^M_{\alpha 4}U^{M*}_{\beta 4}U^{M*}_{\alpha 5}U^M_{\beta 5})$.

For the three active and two sterile neutrino framework we have 4 independent mass squared differences and hence can have the following possibilities for the mass spectrum which we call [14]:

$$\text{N2} + \text{N3}: \quad \Delta m^2_{31} > 0, \quad \Delta m^2_{41} > 0 \text{ and } \Delta m^2_{51} > 0 \,, \quad (40)$$

$$\text{N2} + \text{I3}: \quad \Delta m^2_{31} < 0, \quad \Delta m^2_{41} > 0 \text{ and } \Delta m^2_{51} > 0 \,, \quad (41)$$
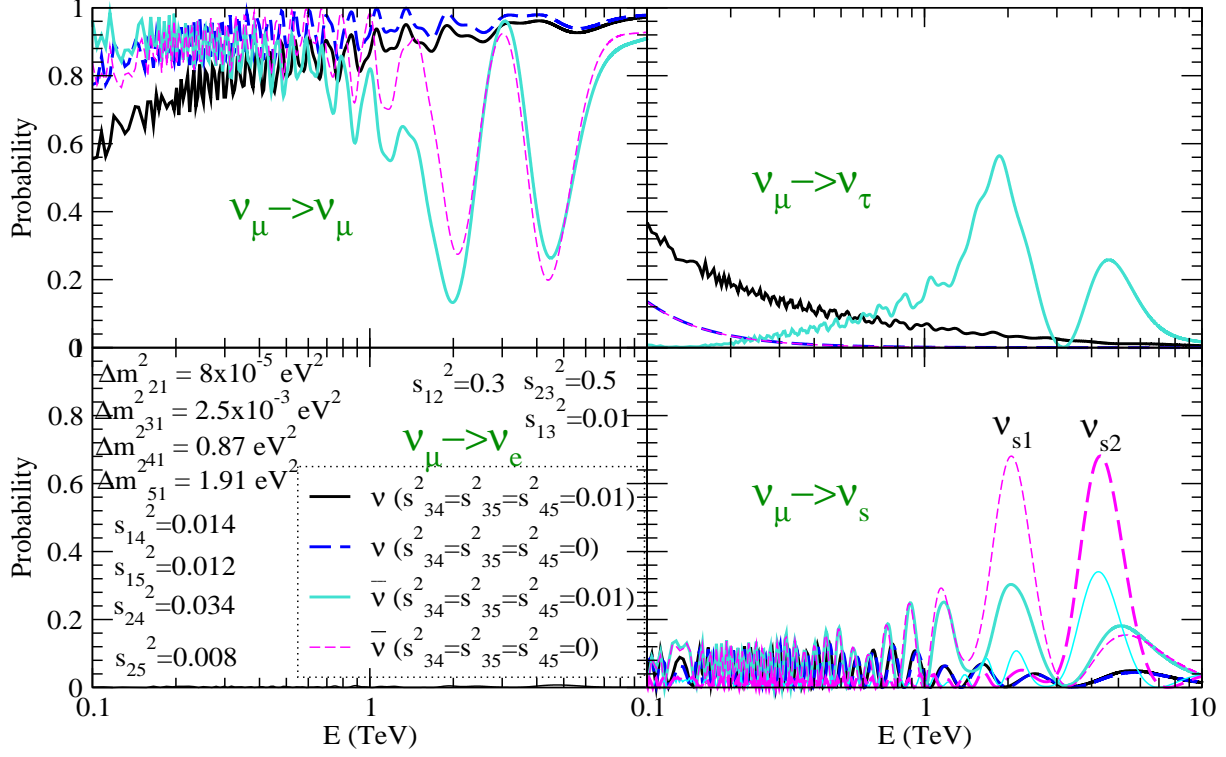
Figure 9: Same as Fig. 8 but for $\Delta m_{41}^2 = +0.87$ eV$^2$ and $\Delta m_{51}^2 = +1.91$ eV$^2$. For $\nu_\mu \to \nu_s$, we show the $\nu_\mu \to \nu_{s1}$ by thin line and $\nu_\mu \to \nu_{s2}$ by thick line.

$$\text{H2} + \text{N3(a)}: \quad \Delta m_{31}^2 > 0, \quad \Delta m_{41}^2 > 0 \text{ and } \Delta m_{51}^2 < 0 \,, \tag{42}$$

$$\text{H2} + \text{I3(a)}: \quad \Delta m_{31}^2 < 0, \quad \Delta m_{41}^2 > 0 \text{ and } \Delta m_{51}^2 < 0 \,, \tag{43}$$

$$\text{I2} + \text{N3}: \quad \Delta m_{31}^2 > 0, \quad \Delta m_{41}^2 < 0 \text{ and } \Delta m_{51}^2 < 0 \,, \tag{44}$$

$$\text{I2} + \text{I3}: \quad \Delta m_{31}^2 < 0, \quad \Delta m_{41}^2 < 0 \text{ and } \Delta m_{51}^2 < 0 \,, \tag{45}$$

with $\Delta m_{21}^2 > 0$ always. In addition, the H2+N3 and H2+I3 schemes can have 2 more possibilities [15]

$$\text{H2} + \text{N3(b)}: \quad \Delta m_{31}^2 > 0, \quad \Delta m_{41}^2 < 0 \text{ and } \Delta m_{51}^2 > 0 \,, \tag{46}$$

$$\text{H2} + \text{I3(b)}: \quad \Delta m_{31}^2 < 0, \quad \Delta m_{41}^2 < 0 \text{ and } \Delta m_{51}^2 > 0 \,. \tag{47}$$

Since there are two mass squared difference associated with the sterile states, we expect two resonances. Whether the resonance occurs in the neutrino or the antineutrino channel depends on the mass ordering. While the ordering of the mass states within the three active part is almost inconsequential for the very high energy neutrinos we are concerned with here, the mass ordering of the sterile states between themselves and with respect to the three active states is of utmost importance. In particular, if both $\Delta m_{41}^2 > 0$ and $\Delta m_{51}^2 > 0$ (corresponding to the N2+N3 and
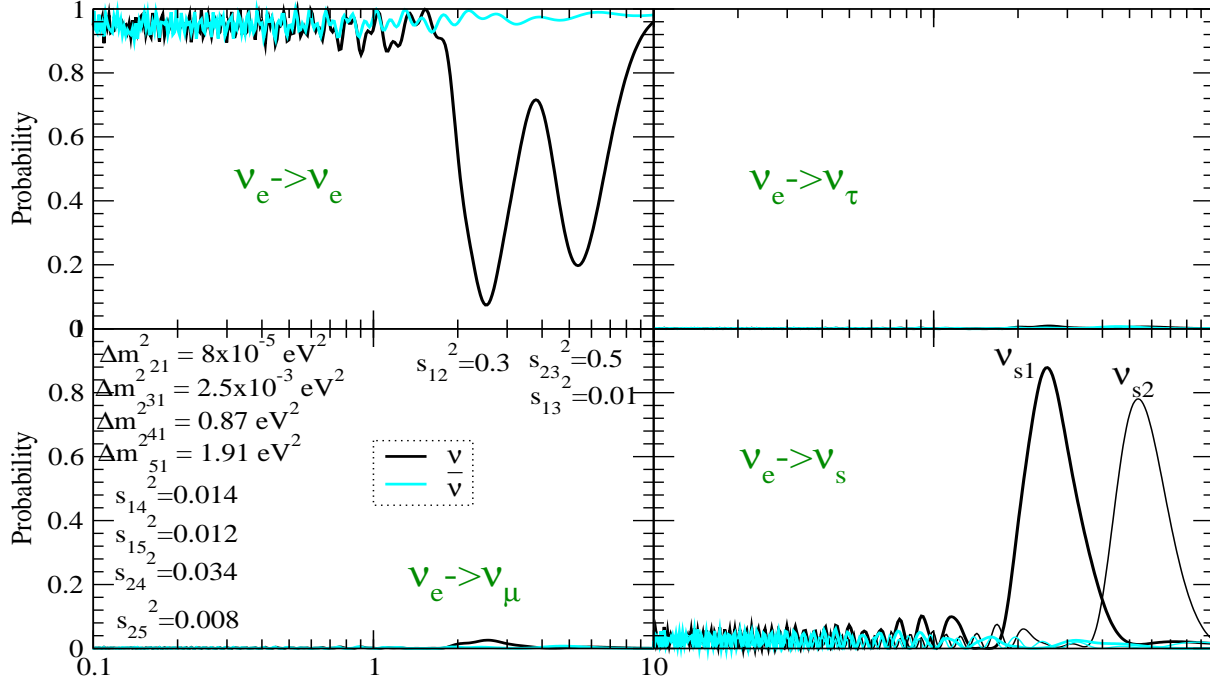
17

Figure 10: The $\nu_e \to \nu_e$ (upper left hand panel), $\nu_e \to \nu_\tau$ (upper right hand panel), $\nu_e \to \nu_\mu$ (lower left hand panel), and $\nu_e \to \nu_{s1}$ and $\nu_e \to \nu_{s2}$ (lower right hand panel) oscillation probabilities, as a function of the neutrino energy $E$ for the 3+2 mass spectrum, when the neutrinos travel a distance $L = 2R_e$, where $R_e$ is the radius of the Earth. The solid black lines show the probabilities for neutrinos while the solid cyan lines are for the antineutrinos. For $\nu_e \to \nu_s$, we show the $\nu_e \to \nu_{s1}$ by thick line and $\nu_e \to \nu_{s2}$ by thin line. We have taken $\Delta m_{41}^2 = 0.87$ eV$^2$ and $\Delta m_{51}^2 = 1.91$ eV$^2$. The oscillation probabilities mainly depend on only $\sin^2\theta_{14}$ and $\sin^2\theta_{15}$ and almost independent of all other mixing angles.

N2+I3 spectra), then both the $\nu_\mu \to \nu_s$ ($\nu_e \to \nu_s$) resonances happen in the antineutrino (neutrino) channel. On the other hand, if both $\Delta m_{41}^2 < 0$ and $\Delta m_{51}^2 < 0$ (corresponding to the I2+N3 and I2+I3 spectra), then both the $\nu_\mu \to \nu_s$ ($\nu_e \to \nu_s$) resonances happen in the neutrino (antineutrino) channel. For the hybrid cases, where $\Delta m_{41}^2 > 0$ and $\Delta m_{51}^2 < 0$ (H2+N3(a) and H2+I3(a)) or $\Delta m_{41}^2 < 0$ and $\Delta m_{51}^2 > 0$ (H2+N3(b) and H2+I3(b)), one of the resonances occur in the neutrino and another in the antineutrino channel.

Figs. 8 and 9 show the probabilities involving the muon (anti)neutrino, as a function of energy for the I2+N3 and N2+N3 cases respectively. The solid black (dark) and dashed blue (dark) lines are for neutrinos and solid cyan (light) and dashed magenta (light) lines are for antineutrinos. We show results for the global best-fit parameter values taken from [12]. When the entire MiniBooNE data is included in the analysis, the authors of [12] get as their best-fit $|\Delta m_{41}^2| = 0.87$ eV$^2$ and $|\Delta m_{51}^2| = 1.91$ eV$^2$ for the mass squared difference and $|U_{e4}| = 0.12$, $|U_{e5}| = 0.11$, $|U_{\mu4}| = 0.18$ and

$|U_{\mu5|} = 0.089$. If we assume a parameterization for the $5 \times 5$ mixing matrix as

$$U = R(\theta_{45})R(\theta_{35})R(\theta_{34})R(\theta_{25})R(\theta_{24})R(\theta_{15})R(\theta_{14})R(\theta_{23})R(\theta_{13})R(\theta_{12}) \ , \qquad (48)$$

then the best-fit values for the matrix elements mentioned above can be obtained if we take $\sin^2 \theta_{14} = 0.014$, $\sin^2 \theta_{15} = 0.012$, $\sin^2 \theta_{24} = 0.034$ and $\sin^2 \theta_{25} = 0.008$. We present our results assuming these values. The other mixing angles associated with the sterile states are $\sin^2 \theta_{34}$, $\sin^2 \theta_{35}$ and $\sin^2 \theta_{45}$. These remain almost unconstrained by the current neutrino oscillation data and could in principle take any value. For the sake of illustration, we show results only for two sets of choices for these mixing angles. The solid lines show probabilities for $\sin^2 \theta_{34} = \sin^2 \theta_{35} = \sin^2 \theta_{45} = 0.01$, while the dashed lines are for $\sin^2 \theta_{34} = \sin^2 \theta_{35} = \sin^2 \theta_{45} = 0.0$. The other mixing angles are fixed at $\sin^2 \theta_{12} = 0.3$, $\sin^2 \theta_{23} = 0.5$ and $\sin^2 \theta_{13} = 0.01$. We see that for the I2+N3 spectrum both resonances are in the neutrino channel while for the N2+I3 spectrum both resonances are in the antineutrino channel. We see that the effect of the mixing angles $\sin^2 \theta_{34}$ and $\sin^2 \theta_{35}$ is to increase the $\nu_\mu \rightarrow \nu_\tau$ oscillations and reduce the $\nu_\mu \rightarrow \nu_s$ transitions in the resonant channel. The net result of these mixing angles is to reduce slightly the net $\nu_\mu$ survival probability. These features are similar to what we had observed for non-zero $\sin^2 \theta_{34}$ for the 3+1 case discussed in the previous section. The reason why $P_{\mu e}$ is very small is easy to see from Eq. (39). In the neutrino channel, say, with $\Delta m^2_{41} < 0$ and $\Delta m^2_{51} < 0$ as in Fig. 8, while $U^M_{\mu 4}$ and $U^M_{\mu 5}$ increase due to resonance, $U^M_{e4}$ and $U^M_{e5}$ remain negligible since $\theta^M_{14}$ remains small, and as a result $P_{\mu e}$ remains negligible. In the antineutrino channel for this mass spectrum $U^M_{e4}$ and $U^M_{e5}$ are large (as discussed below), however in that case $U^M_{\mu 4}$ and $U^M_{\mu 5}$ are small. Therefore, $P_{\mu e}$ is always small. Similarly, using Eq. (39) it is easy to see that $P_{\mu\tau}$ is large when $\sin^2 \theta_{34}$ and $\sin^2 \theta_{35}$ are large. In fact, its easy to see that non-zero $\sin^2 \theta_{34}$ brings the $\Delta m^2_{41}$ driven first peak in $P_{\mu\tau}$ and non-zero $\sin^2 \theta_{35}$ brings the $\Delta m^2_{51}$ driven second peak. Using similar arguments one can check that the muon neutrinos oscillate into the first sterile neutrino at the $\Delta m^2_{41}$ driven resonance and into the second sterile neutrino at the $\Delta m^2_{51}$ driven resonance.

Since the mixing angle $\sin^2 \theta_{14}$ is non-zero, we expect resonant transitions for electron neutrinos as well. We show in Fig. 10 the oscillation probabilities associated with the electron type neutrinos and antineutrinos. The upper left hand panel shows the survival probability $P_{ee}$, the upper right hand panel shows $P_{e\tau}$, the lower left hand panel shows $P_{e\mu}$, while the lower right hand panel shows the transition probability to the first sterile state, $P_{es_1}$ and to the second sterile state, $P_{es_2}$. We have assumed the N2+N3 (or N2+I3) spectrum for the neutrinos with the current global best-fit numbers for the oscillation parameters. The black (dark) lines are for neutrinos while the cyan (light) lines are for antineutrinos. For the I2+N3 (and I2+I3) spectra, the black (dark) lines would be for antineutrinos and cyan (light) lines for neutrinos. As discussed before, we see that both resonances come in the neutrino (antineutrino) channel when $\Delta m^2_{41} > 0$ and $\Delta m^2_{51} > 0$ ($\Delta m^2_{41} < 0$ and $\Delta m^2_{51} < 0$). For the hybrid cases H2+N3(a) and H2+N3(b) (as well as H2+I3(a) and H2+I3(b)), only one resonance will occur in either the neutrino or the antineutrino channel depending whether the mass squared difference is positive or negative respectively.

The expressions for the probabilities involving the electron neutrino in the 3+2 picture using the parameterization for $U$ given by Eq. (48) are

$$P_{ee} \simeq 1 \quad - \quad \cos^4 \theta^M_{15} \sin^2 2\theta^M_{14} \sin^2 \left[ \frac{(\Delta m^2_{41})^M L}{4E} \right]$$

19

$$
\begin{aligned}
- \quad & \cos^2 \theta_{14}^M \sin^2 2\theta_{15}^M \sin^2 \left[ \frac{(\Delta m_{51}^2)^M L}{4E} \right] \\
- \quad & \sin^2 \theta_{14}^M \sin^2 2\theta_{15}^M \sin^2 \left[ \frac{(\Delta m_{54}^2)^M L}{4E} \right].
\end{aligned}
\tag{49}
$$

The mixing angles $\sin^2 \theta_{14}^M$ and $\sin^2 \theta_{15}^M$ do not reach maximal value simultaneously. Therefore, we can see from this expression that we would have 2 big dips in the survival probability due to the first and the second terms when we have the $\Delta m_{41}^2$ and $\Delta m_{51}^2$ driven resonances respectively. The last term is proportional to $\sin^2 \theta_{14}^M \sin^2 2\theta_{15}^M$ and needs $\theta_{14}^M$ and and $\theta_{15}^M$ to be large simultaneously. A third dip would be possible only when this condition is satisfied. The transition probabilities have the general form given by Eq. (39). The reason why $P_{e\mu} \simeq 0$ and $P_{e\tau} \simeq 0$ is same as that discussed before. If the $\nu_e \rightarrow \nu_s$ resonance happens in the neutrino channel, the $\nu_\mu \rightarrow \nu_s$ resonance will happen in the antineutrino channel. Therefore, when $\sin^2 \theta_{14}^M = 1$ or $\sin^2 \theta_{15}^M = 1$ due to $\nu_e \rightarrow \nu_s$ resonance, the other mixing angles do not receive any matter enhancement. One can check that in this case the mixing matrix elements $U_{\mu 4}^M$, $U_{\mu 5}^M$, $U_{\tau 4}^M$ and $U_{\tau 5}^M$ are very small if the sterile mixing angles in vacuum are small and we have $P_{e\mu} \simeq 0$ and $P_{e\tau} \simeq 0$.

## 5    Flavor and Event Ratios with Sterile Neutrinos

Neutrino telescopes, such as IceCube and Km3Net are not expected to have any charge identification capability. Therefore, they will not be able to distinguish the neutrino signal from the antineutrino signal. This is particularly relevant for matter effects, since resonant transitions due to Earth matter is large in only either the neutrino or the antineutrino channel for a given sign of the mass squared difference which drives the resonance. Consequently, one should look at the sum of the neutrino and antineutrino events expected at the neutrino telescope. The threshold energies for muon, electron and tau detection in IceCube are about 100 GeV, 1 TeV and 1000 TeV, respectively. It is easiest to see muon events, which leave distinct tracks in the detector. Both the electron events and the tau events produce showers. In principle the tau events should be separable from the electron events in certain energy range where they produce the so-called "double bang" signal in the detector [37]. However, because tau events have energy threshold of about 1000 TeV, they are not of any interest to us. Therefore, we could consider the simple event ratio

$$
r = \frac{N_{\nu_\mu} + N_{\bar{\nu}_\mu}}{N_{\nu_e} + N_{\bar{\nu}_e}} \ ,
\tag{50}
$$

where $N_\alpha$ are the number of events observed corresponding to the species type $\alpha$. The number of events is mainly given in terms of the (anti)neutrino flux, cross-section and the relevant oscillation probabilities. A detail prescription for calculating the number of events due to atmospheric $\nu_\mu$ is given in [26]. In this paper, we will not attempt to calculate the number of events exactly, which in addition to the main quantities mentioned above, also depend on other things like distance covered and energy loss of the lepton inside ice, details of the detector and the necessary cuts of the experiment. Instead, just for the purpose of illustration, we present the ratio of the product
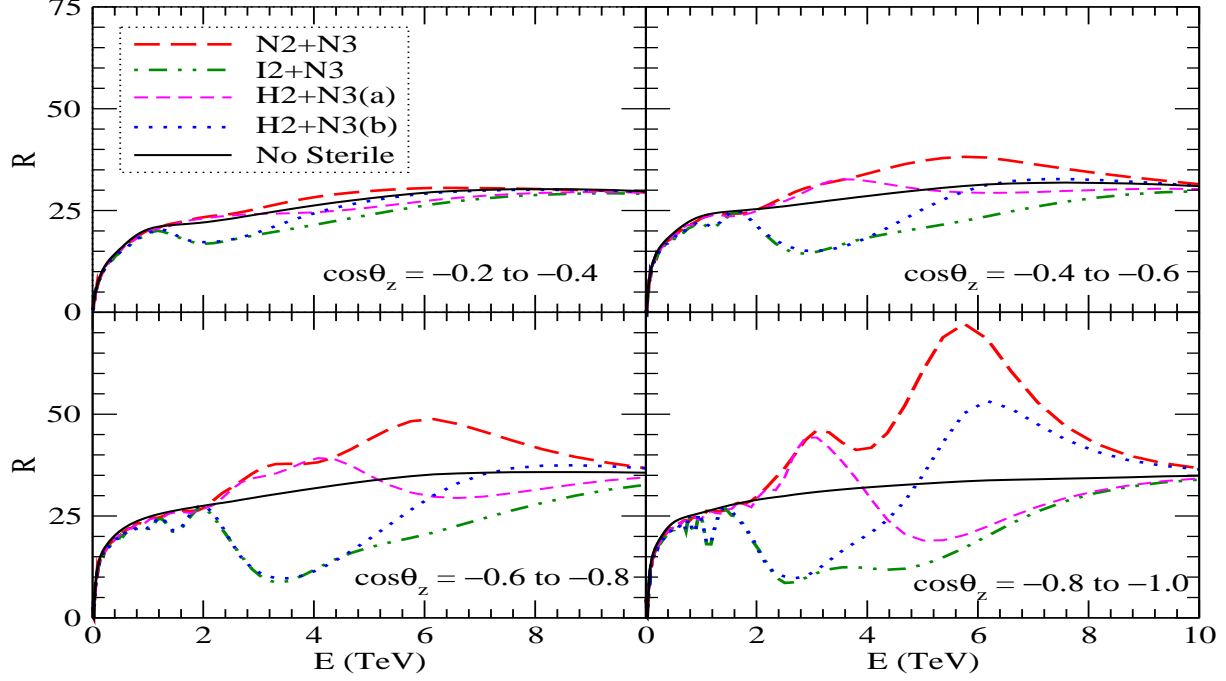
Figure 11: Binned result for the ratio $R$ as a function of energy $E$. The upper left panel shows the result for the zenith bin $-0.2 \geq \cos\theta_z \geq -0.4$, the upper right panel for $-0.4 \geq \cos\theta_z \geq -0.6$, the lower left panel for $-0.6 \geq \cos\theta_z \geq -0.8$, and the lower right panel for $-0.8 \geq \cos\theta_z \geq -1.0$. The solid lines show the expected $R$ in the respective zenith bins when we have no sterile neutrinos and there are only three generation oscillations. The other 4 line types correspond to N2+N3 (long dashed red lines), I2+I3 (dot-dashed green lines), H2+N3(a) (dashed magenta lines) and H2+N3(b) (dotted blue lines). For all cases we have taken $|\Delta m^2_{41}| = 0.87$ eV$^2$, $|\Delta m^2_{51}| = 1.91$ eV$^2$ and mixing angles corresponding to their global best-fit values. We take $\sin^2\theta_{34} = \sin^2\theta_{35} = \sin^2\theta_{45} = 0.01$.

of the flux, cross-section and the relevant probabilities as

$$R = \frac{[\phi_{\nu_\mu}P_{\mu\mu} + \phi_{\nu_e}P_{e\mu}]\sigma_\nu + [\phi_{\bar{\nu}_\mu}P_{\bar{\mu}\bar{\mu}} + P_{\bar{e}\bar{\mu}}]\sigma_{\bar{\nu}}}{[\phi_{\nu_e}P_{ee} + \phi_{\nu_\mu}P_{\mu e}]\sigma_\nu + [\phi_{\bar{\nu}_e}P_{\bar{e}\bar{e}} + \phi_{\bar{\nu}_\mu}P_{\bar{\mu}\bar{e}}]\sigma_{\bar{\nu}}} \ . \tag{51}$$

We use the atmospheric neutrino flux given by Honda *et. al.* [38] and high energy charged current cross-sections from [39]. The efficiency of observing electron events is smaller than for muon events. However the difference in the $1-10$ TeV range is small and therefore we neglect that here, since what we present is merely for illustration only. IceCube is expected to have rather good zenith angle resolution of about $25°$ [40] and in [26] the authors have presented their results in 5 energy bins between $1-10$ TeV. In Fig. 11 we show the zenith angle binned value for $R$, as a function of the energy $E$. We have divided the zenith angle range $-0.2 \geq \cos\theta_z \geq -1.0$, into 4 bins and show results where we have calculated $R$ by summing over the product of the flux,

cross-section and relevant probabilities in the zenith bins. The upper left panel shows the result for the zenith bin $-0.2 \geq \cos\theta_z \geq -0.4$, the upper right panel for $-0.4 \geq \cos\theta_z \geq -0.6$, the lower left panel for $-0.6 \geq \cos\theta_z \geq -0.8$, and the lower right panel for $-0.8 \geq \cos\theta_z \geq -1.0$. The solid black lines show the expected $R$ in the respective zenith bins when we have no sterile neutrinos and there are only three generation oscillations. Note that these three generation oscillations are important for neutrino energies up to 1 TeV for neutrinos travelling large distances inside Earth. The other 4 line types correspond to the 4 relevant mass spectra discussed for the 3+2 scheme, N2+N3 (long dashed red lines), I2+I3 (dot-dashed green lines), H2+N3(a) (dashed magenta lines) and H2+N3(b) (dotted blue lines). For all cases we have taken $|\Delta m^2_{41}| = 0.87$ eV$^2$, $|\Delta m^2_{51}| = 1.91$ eV$^2$ and mixing angles corresponding to their global best-fit values, as discussed in Section 4. The hitherto unconstrained mixing angles $\sin^2\theta_{34}$, $\sin^2\theta_{35}$ and $\sin^2\theta_{45}$ are taken as 0.01. We see that there is a huge change in the value of $R$ due to presence of sterile neutrinos for all values of $E$ between 1 and 10 TeV. The change is also seen to be clearly dependent on the energy and zenith angle of the neutrinos. We note from the figure that not only should it be possible to establish the presence of sterile neutrinos from the observations, it should also be possible to differentiate between the different 3+2 neutrino mass because each one of them has a distinct prediction for $R$.

Few comments are in order. The number of muon events expected from high energy atmospheric neutrinos has been given in Table 1 of [26], for 2 zenith angle bins $-0.6 \geq \cos\theta_z \geq -1.0$ and $-0.2 \geq \cos\theta_z \geq -0.6$ and different energy bins. In the $-0.6 \geq \cos\theta_z \geq -1.0$ bin, about 52,474 muon events are expected in $0.1 \leq E$ (TeV) $\leq 0.16$ energy bin, about 3,330 events in $0.25 \leq E$ (TeV) $\leq 3.98$ energy bin and about 1,721 events in $3.98 \leq E$ (TeV) $\leq 6.31$ energy bin, after 10 years of IceCube operation. Higher number of events are expected in the $-0.2 \geq \cos\theta_z \geq -0.6$ zenith angle bin. Thus we expect a rather good statistic atmospheric neutrino data at the neutrino telescopes. In fact, with such high statistic, it should be possible to look for sterile neutrinos in the atmospheric neutrino data sample using just the muon events alone.

# 6  Conclusions

Following the recently declared MiniBooNE results, sterile neutrinos have been the focus of discussions in the field of neutrino physics. In particular, the question whether MiniBooNE data has unambiguously ruled out the possibility of sterile neutrinos needed to explain the LSND results has been raised. In this paper we have expounded the possibility of answering this question using the high energy atmospheric neutrino data in the upcoming neutrino telescopes.

If sterile neutrinos exist with $\Delta m^2 \sim$ eV$^2$, we expect to see flavor oscillations of upward going atmospheric neutrinos with the peak in the transition probability at an energy of a few TeV. One could naively think that these oscillations would normally be small owing to the smallness of the sterile mixing angles, which are severely constrained by the short baseline oscillation experiment data. We pointed out that near-resonant matter effects driven by the sterile neutrino mass squared differences drive these very small mixing angles in vacuum to almost maximal in matter. For a given neutrino baseline inside the Earth, the largest oscillations of course occur when the condition of resonance and the condition of oscillation peak are simultaneously satisfied. We showed in the framework of the simpler 3+1 neutrino mass scenario that this condition could be satisfied for TeV

neutrinos crossing the Earth. We assumed a simple framework where the only non-zero sterile angle was $\theta_{24}$ and calculated the value of the mixing angle for which one could have maximal $\nu_\mu$ oscillations into sterile neutrino. For $\theta_{24}$ both larger and smaller than this critical value, one would get lesser oscillation. We next allowed for non-zero $\theta_{34}$ values and studied how this mixing angle changed the oscillation scenario. We showed that matter effects simultaneously enhance both $\theta_{24}$ and $\theta_{34}$ and we have genuine three generation effects in the oscillation probability. One very important effect is that with non-zero $\theta_{34}$ the $P_{\mu\tau}$ oscillation probability increases significantly and could even become maximal, while the $P_{\mu s}$ probability simultaneously decreases.

We considered the still viable 3+2 neutrino mass and mixing scheme and presented the oscillation probabilities when all mixing angles were allowed to be non-zero, as needed to explain the global oscillation data, including LSND and MiniBooNE. For the 3+2 mass scheme one can have as many as 8 different mass ordering. Of these, there are at least 4 different possibilities that would allow for resonant matter transition driven by the sterile mass eigenstates and each one gives a distinct signature in the oscillation pattern. We presented the results for the oscillation probabilities obtained by evolving the full five generation neutrino system inside the Earth matter as they travel, assuming the PREM profile for the matter density. We explained these results using simplified constant matter density picture. We showed that the mixing angles $\theta_{34}$ and $\theta_{35}$ which are enhanced inside the Earth matter cause $P_{\mu\tau}$ to increase significantly. We emphasized the fact that while $\nu_\mu \to \nu_s$ resonance occurs for $\Delta m^2 < 0$ in the neutrino channel, the $\nu_e \to \nu_s$ resonance condition is satisfied for $\Delta m^2 > 0$ in the neutrino channel. In the antineutrino channel of course the sign of $\Delta m^2$ is reversed for the resonance condition to be satisfied. We showed how this feature ensured that the transition probability $P_{e\mu}$ and $P_{e\tau}$ always remained negligible. For $\theta_{14}$ and/or $\theta_{15}$ non-zero, we showed how resonance in the neutrino (antineutrino) channel produces huge dips in $P_{ee}$.

Finally, we discussed how these large matter effects due to presence of sterile neutrinos would show up in the neutrino telescopes. Atmospheric neutrinos form a "background" for the ultra high energy neutrino observation in the neutrino telescopes. These atmospheric neutrinos are in the TeV range where we expect near-resonant matter effects. At these energies hundreds of thousands of muon type events are expected from atmospheric neutrinos in IceCube and we argued that even a very moderate energy and zenith angle resolution in the data would lead to an unambiguous signal for sterile neutrinos.

## Note Added

After the first version of the this paper appeared, the Super-Kamiokande collaboration have released their data on showering muon events, which come from neutrinos with energies in the TeV range [41]. They comment on the feasibility of using their very high energy upward-going muon data sample which come from showing type events to shed light on the existence of high $\Delta m^2$ solutions, and cite this paper.

# References

[1] Y. Ashie *et al.* [Super-Kamiokande Collaboration], Phys. Rev. D **71**, 112005 (2005).

[2] B. T. Cleveland *et al.*, Astrophys. J. **496**, 505 (1998); J. N. Abdurashitov *et al.* [SAGE Collaboration], J. Exp. Theor. Phys. **95**, 181 (2002) [Zh. Eksp. Teor. Fiz. **122**, 211 (2002)]; W. Hampel *et al.* [GALLEX Collaboration], Phys. Lett. B **447**, 127 (1999); S. Fukuda *et al.* [Super-Kamiokande Collaboration], Phys. Lett. B **539**, 179 (2002); B. Aharmim *et al.* [SNO Collaboration], Phys. Rev. C **72**, 055502 (2005); Borexino Collaboration, arXiv:0708.2251 [astro-ph].

[3] M. C. Gonzalez-Garcia and M. Maltoni, arXiv:0704.1800 [hep-ph]. M. Maltoni, T. Schwetz, M. A. Tortola and J. W. F. Valle, New J. Phys. **6**, 122 (2004), hep-ph/0405172; S. Choubey, Phys. Atom. Nucl. **69**, 1930 (2006); S. Goswami, Int. J. Mod. Phys. A **21**, 1901 (2006); S. Goswami, A. Bandyopadhyay and S. Choubey, Nucl. Phys. Proc. Suppl. **143**, 121 (2005); A. Bandyopadhyay, S. Choubey, S. Goswami, S. T. Petcov and D. P. Roy, Phys. Lett. B **608**, 115 (2005); G. L. Fogli, E. Lisi, A. Marrone and A. Palazzo, Prog. Part. Nucl. Phys. **57**, 742 (2006).

[4] T. Araki *et al.* [KamLAND Collaboration], Phys. Rev. Lett. **94**, 081801 (2005).

[5] E. Aliu *et al.* [K2K Collaboration], Phys. Rev. Lett. **94**, 081802 (2005).

[6] D. G. Michael *et al.*, [MINOS Collaboration], arXiv:hep-ex/0607088.

[7] M. Apollonio *et al.*, Eur. Phys. J. C **27**, 331 (2003).

[8] A. A. Aguilar-Arevalo *et al.* [The MiniBooNE Collaboration], arXiv:0704.1500.

[9] C. Athanassopoulos *et al.*, (The LSND Collaboration) Phys. Rev. Lett. **77**, 3082 (1996); C. Athanassopoulos *et al.*, (The LSND Collaboration) Phys. Rev. Lett. **81**, 1774 (1998).

[10] Y. Declais *et al.*, Phys. Lett. B **338**, 383 (1994); F. Dydak *et al.*, Phys. Lett. B **134**, 281 (1984); I. E. Stockdale *et al.*, Phys. Rev. Lett. **52**, 1384 (1984); B. Armbruster *et al.* [KARMEN Collaboration], Phys. Rev. D **65**, 112001 (2002); P. Astier *et al.* [NOMAD Collaboration], Phys. Lett. B **570**, 19 (2003).

[11] J. J. Gomez-Cadenas and M. C. Gonzalez-Garcia, Z. Phys. C **71**, 443 (1996); S. Goswami, Phys. Rev. D **55**, 2931 (1997). S. M. Bilenky, C. Giunti and W. Grimus, Eur. Phys. J. C **1**, 247 (1998).

[12] M. Maltoni and T. Schwetz, arXiv:0705.0107 [hep-ph].

[13] M. Sorel, J. M. Conrad and M. H. Shaevitz, Phys. Rev. D **70**, 073004 (2004).

[14] S. Choubey, N. P. Harries, and G. G. Ross, Phys. Rev. D **74**, 053010 (2006). S. Choubey, N. P. Harries and G. G. Ross, arXiv:hep-ph/0703092.

[15] S. Goswami and W. Rodejohann, arXiv:0706.1462 [hep-ph].

[16] G. Karagiorgi, talk at NuFact07, Okayama University, Okayama, Japan, August 6 – 11, 2007.
*http://fphy.hep.okayama-u.ac.jp/nufact07/program/*

[17] A. Bandyopadhyay and S. Choubey, arXiv:0707.2481 [hep-ph].

[18] A. Donini, M. Maltoni, D. Meloni, P. Migliozzi and F. Terranova, arXiv:0704.0388 [hep-ph].

[19] A. Dighe and S. Ray, arXiv:0709.0383 [hep-ph].

[20] R. L. Awasthi and S. Choubey, arXiv:0706.0399 [hep-ph].

[21] A. Achterberg *et al.* [IceCube Collaboration], arXiv:astro-ph/0604450; S. R. Klein[for the IceCube Collaboration], arXiv:astro-ph/0601269. K. Rawlins *et al.* [IceCube Collaboration], "IceCube: A Multipurpose Neutrino Telescope" http://icecube.wisc.edu

[22] U. F. Katz, Nucl. Instrum. Meth. A **567**, 457 (2006) [arXiv:astro-ph/0606068].

[23] P. Piattelli [NEMO Collaboration], Nucl. Phys. Proc. Suppl. **143**, 359 (2005).

[24] L. K. Resvanis *et al.* [NESTOR Collaboration], Nucl. Phys. Proc. Suppl. **35**, 294 (1994).

[25] J. Ahrens *et al.* [AMANDA Collaboration], Phys. Rev. D **66**, 012005 (2002).

[26] M. C. Gonzalez-Garcia, F. Halzen and M. Maltoni, Phys. Rev. D **71**, 093010 (2005).

[27] D. Morgan, E. Winstanley, J. Brunner and L. F. Thompson, arXiv:0705.1897 [astro-ph]; D. Hooper, D. Morgan and E. Winstanley, Phys. Lett. B **609**, 206 (2005).

[28] A. Nicolaidis, G. Tsirigoti and J. Hansson, arXiv:hep-ph/9904415.

[29] O. Yasuda, arXiv:hep-ph/0102166.

[30] H. Nunokawa, O. L. G. Peres and R. Zukanovich Funchal, Phys. Lett. B **562**, 279 (2003).

[31] L. Wolfenstein, Phys. Rev. D **17**, 2369 (1978).

[32] S. P. Mikheev and A. Y. Smirnov, Sov. J. Nucl. Phys. **42**, 913 (1985) [Yad. Fiz. **42**, 1441 (1985)]; S. P. Mikheev and A. Y. Smirnov, Nuovo Cim. C **9**, 17 (1986).

[33] V. D. Barger, K. Whisnant, S. Pakvasa and R. J. N. Phillips, Phys. Rev. D **22**, 2718 (1980).

[34] A. M. Dziewonski and D. L. Anderson, Phys. Earth Planet. Interiors **25**, 297 (1981); S. V. Panasyuk, Reference Earth Model (REM) webpage, http://cfauves5.harvrd.edu/lana/rem/index.html.

[35] R. Gandhi, P. Ghoshal, S. Goswami, P. Mehta and S. Uma Sankar, Phys. Rev. Lett. **94**, 051801 (2005); R. Gandhi, P. Ghoshal, S. Goswami, P. Mehta and S. Uma Sankar, Phys. Rev. D **73**, 053001 (2006); S. K. Agarwalla, S. Choubey, S. Goswami and A. Raychaudhuri, Phys. Rev. D **75**, 097302 (2007); E. K. Akhmedov, M. Maltoni and A. Y. Smirnov, JHEP **0705**, 077 (2007).

[36] S. K. Agarwalla, S. Choubey and A. Raychaudhuri, Nucl. Phys. B **771**, 1 (2007).

[37] J. G. Learned and S. Pakvasa, Astropart. Phys. **3**, 267 (1995).

[38] M. Honda *et al.*, Phys. Rev. D **70**, 043008 (2004).

[39] R. Gandhi, C. Quigg, M. H. Reno and I. Sarcevic, Phys. Rev. D **58**, 093009 (1998); R. Gandhi, C. Quigg, M. H. Reno and I. Sarcevic, Astropart. Phys. **5**, 81 (1996).

[40] J. F. Beacom, N. F. Bell, D. Hooper, S. Pakvasa and T. J. Weiler, Phys. Rev. D **68**, 093005 (2003) [Erratum-ibid. D **72**, 019901 (2005)].

[41] S. Desai *et al.* [Super-Kamiokande Collaboration], arXiv:0711.0053 [hep-ex].